sustainability

MDPI

Article

Efficiency Maximization of Grid-Connected Tidal Stream Turbine System: A Supervisory Energy-Based Speed Control Approach with Processor in the Loop Experiment

Youcef Belkhier [1], Nasim Ullah [2,*] and Ahmad Aziz Al Alahmadi [2]

[1] Laboratoire de Technologie Industrielle et de l'Information (LTII), Faculté de Technologie, Université de Bejaia, Bejaia 06000, Algeria; youcef.belkhier@univ-bejaia.dz
[2] Department of Electrical Engineering, College of Engineering, Taif University, P.O. Box 11099, Taif 21944, Saudi Arabia; aziz@tu.edu.sa
* Correspondence: nasimullah@tu.edu.sa

Abstract: Permanent magnet synchronous generator (PMSG) with a back-to-back power converter is one of the commonly used technologies in tidal power generation schemes. However, the nonlinear dynamics and time-varying parameters of this kind of conversion system make the controller computation a challenging task. In the present paper, a novel intelligent control method based on the passivity concept with a simple structure is proposed. This proposed strategy consists of passivity-based speed control (PBSC) combined with a fuzzy logic method to address the robustness problems faced by conventional control techniques such as proportional-integral (PI) control. The proposed method extracts the maximum power from the tidal energy, compensates for the uncertainty in a damped way where the entire dynamics of the PMSG are considered when designing the control law. The fuzzy logic controller is selected, which makes the proposed strategy intelligent to compute the damping gains to make the closed-loop passive and approximate the unstructured dynamics of the PMSG. Thus, the robustness property of the closed-loop system is considerably increased. The regulation of DC voltage and reactive power to their desired values are the principal objectives of the present work. The proposed method is used to control the machine-side converter (MSC), while a conventional PI method is adopted to control the grid-side converter (GSC). Dynamic simulations show that the DC voltage and reactive power errors are extremely reduced with the proposed strategy; ± 0.002 for the DC-link voltage and ± 0.000015 in the case of the reactive power. Moreover, the lowest steady-state error and better convergence criterion are shown by the proposed control (0.3×10^{-3} s). Generally, the proposed candidate offers high robustness, fast speed convergence, and high efficiency over the other benchmark nonlinear strategies. Moreover, the proposed controller was also validated in a processor in the loop (PIL) experiment using Texas Instruments (TI) Launchpad.

Keywords: renewable energy; fuzzy logic controller; energy-based controller; marine current turbine; nonlinear control; processor in the loop experiment

Citation: Belkhier, Y.; Ullah, N.; Al Alahmadi, A.A. Efficiency Maximization of Grid-Connected Tidal Stream Turbine System: A Supervisory Energy-Based Speed Control Approach with Processor in the Loop Experiment. *Sustainability* **2021**, *13*, 10216. https://doi.org/10.3390/su131810216

Academic Editor: Detlef Schulz

Received: 30 July 2021
Accepted: 6 September 2021
Published: 13 September 2021

1. Introduction

The tidal energy that results from the transformation of the kinetic energy of marine currents into electrical energy through tidal turbines has gained increasing attention in recent years due to its advantages of being a clean source of renewable energy and highly predictable, compared to its predecessors [1,2]. Therefore, it is a marine transposition of the wind rotor that recovers the kinetic energy of the wind. The parallel that can be established between the two technologies can be found in the first place in the similar designs that have been adopted. The use of PMSG in tidal turbine systems has high potential due to its reliability, increased energy, reduced failure, and the possibility to eliminate the gearbox, which leads to low maintenance and enables the PMSG to be very favorable in marine current applications [2]. However, the controller computation for the PMSG is still

a challenging task, due to unknown modeling errors, external disturbances, and parameter uncertainties. Furthermore, the DC-link overvoltage control, reactive power support, the efficiency of the power electronics, and ride-through fault capability are important requirements in grid-connected tidal energy systems for reliable and efficient electrical energy [3]. Several research works dedicated to the nonlinear control of PMSG have appeared in the literature and in the industry. In [4], a super twisting algorithm combined with a high-order sliding approach (SMC) is presented. In [5], a sliding mode combined with a jaya-based strategy is proposed. However, the combined strategy increases the costs and maintenance time. A hybrid controller was developed in [6] of a new hydrostatic tidal turbine and a disturbance rejection combined with a backstepping control method was investigated in [7]. However, the authors have not investigated the sudden changes in the behavior of the tidal current and time-varying parameters. The same system was adopted in [8], where the SMC control has been replaced by the proposed novel active disturbance rejection control method (ADRC). The ADRC shows a clear improvement in the control performance compared to that of the SMC and the classical PI controls. A novel Q-network algorithm combined with a Tilt-based fuzzy cascaded strategy is proposed in [9]. An SMC with a magnetic equivalent circuit was developed in [10]. Moreover, the authors have not investigated the robustness of the proposed strategy under time-varying parameters. A linear quadratic control is proposed in [11] with Perturb and the observed algorithm in [12]. Other control strategies that can be adopted for this kind of conversion system are proposed in [13–15]. However, the majority of these controls are signal based and do not take into account the physical structure of the synchronous machine during the controller design, as mentioned in [16].

Within the work, a novel control method, based on the passivity concepts that track velocity and maintain this one while operating at the optimal torque, is proposed. One of the inherent advantages of the passivity-based control (PBC) method, also called "Energy-based control (EBC)" is that the nonlinear properties are not canceled but compensated in a damped way [17,18]. Several kinds of research work about the passivity control dedicated to the PMSG have appeared in the literature and in the industry. A PBC associated with a sliding mode controller is adopted in [19]. However, the proposed strategy uses fixed gains, which are difficult to compute when the system is under parameter uncertainties. In [20], a hybrid PBC, SMC, and fuzzy control have been developed. However, the control design is very complex to implement. The passivity-based linear feedback control is explored in [21]. However, nonlinear properties and the robustness due to parameter changes of the PMSG have not been evaluated. A sampled-data interconnection and damping assignment PBC (IDA-PBC) approach is investigated in [22]. However, in the presented work, external disturbances and parameter changes were not taken into account. The passivity-based speed controller (PBSC) is investigated in [23]. However, the authors have not investigated the robustness of the proposed strategy under time-varying parameters. A passivity-based controller on ADRC combined with the IDA-PBC approach is developed in [24].

To overcome the aforementioned control drawbacks, in the present paper, a novel passivity-based speed control (PBSC) combined with the fuzzy logic control for optimal performance of a PMSG is proposed and for the improvement of the power quality transferred to the grid. The main objectives of this study consist of two main parts: Extracting the maximum marine current power through controlling the rotational of the PMSG and transferring this power to the grid-side converter (GSC). For this, a new controller is proposed. The main hypothesis is to allow the PMSG to operate at the same speed as the marine current turbine. To this end, an optimization way to minimize as much as possible the speed error is investigated through the PMSG speed control. The task of the second objective is to regulate the reactive power and DC-link voltage at their pre-fault values to guarantee efficient, secure, and reliable electricity, and to avoid any possible disturbances related to the MSC such as sudden changes in tidal velocity, parametric uncertainties, and PMSG nonlinear properties. Thus, a classical PI controller is adopted by the GSC that is to enhance the overall performances of the closed-loop. A special focus is given to the

PMSG, as it is the bridge between the tidal turbine and the grid, that is, by keeping into consideration the complete dynamic of the PMSG when formulating the new proposed control plan. Furthermore, the robustness against parameter changes has been given special attention. The novelty and research contribution of this technique is its simple structure and the incredibly low number of fixed gains used by the proposed approach, which reduces the system's sensitivity to measurement noise and greatly improves the system's global stability and robustness. Moreover, the fuzzy logic controller is selected which makes the proposed strategy intelligent to compute the damping gains and approximate the unstructured dynamics of the PMSG. Extensive numerical investigations are made to demonstrate the robustness of the proposed approach against parameter changes and external disturbances. Moreover, extensive comparison with other nonlinear controls is provided to highlight the superiority of the proposed fuzzy supervisory-PBSC (FS-PBSC). Moreover, utilizing the Texas Instruments (TI) Springboard, the suggested controller is validated in a PIL experiment.

This paper is organized in the present form. In Section 2, the system description, the proposed strategy design procedure, and the control method applied to the grid-side converter (GSC) are established. Section 3 deals with the extensive numerical investigation and experimental validation of the proposed candidate strategy. Finally, Section 4 deals with the main conclusions of the present paper.

2. Methods and Materials

2.1. Marine Current Conversion System Modeling

The configuration of the investigated conversion system with MATLAB/Simulink is presented in Figure 1, which is mainly composed of tidal turbine, PMSG, AC-DC-AC converter, and the grid. The proposed strategy is applied to the MSC for regulation of the produced power via the generator, while the network receives only the active power using the classical PI method, which represents the main aim of the GSC controller.

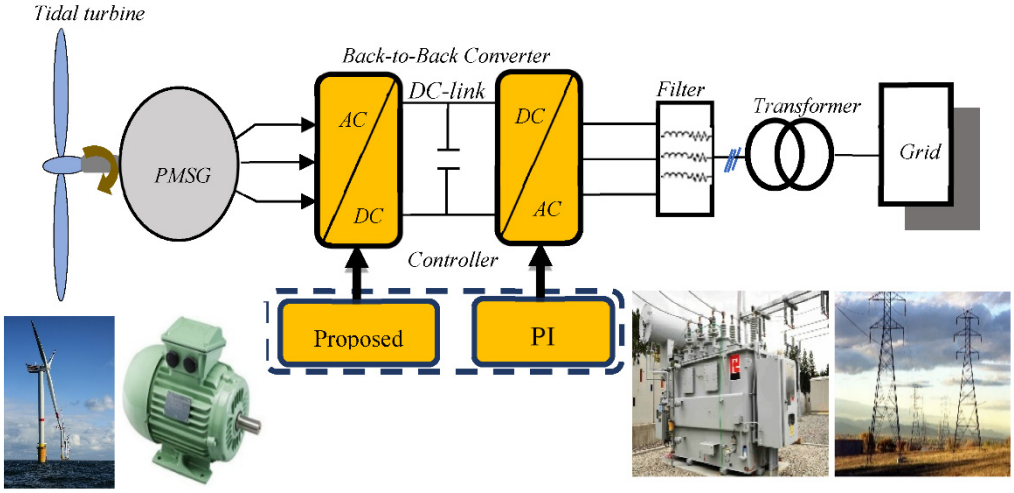

Figure 1. Marine current conversion system.

2.1.1. Tidal Turbine Model

The following is the mathematical formula of the marine current power that can be extracted by the turbine [5,25]:

$$P_m = \frac{1}{2}\rho C_p(\beta,\lambda)Av_s^3, \quad (1)$$

$$T_m = \frac{P_m}{\omega_m}, \quad (2)$$

$$C_p(\beta,\lambda) = 0.5\left(\frac{116}{\lambda_i} - 0.4\beta - 5\right)e^{-\left(\frac{21}{\lambda_i}\right)}, \tag{3}$$

$$\lambda_i^{-1} = (\lambda + 0.08\beta)^{-1} - 0.035\left(1+\beta^3\right)^{-1}, \tag{4}$$

$$\lambda = \frac{\omega_t R}{v_s} \tag{5}$$

where v_s denotes the marine current speed, β denotes the pitch angle, ω_t denotes the turbine speed, R denotes the radius of the blades, C_p represents the power coefficient, λ denotes tip-speed ratio, ρ represents marine current density, and A represents the swept area of the blades.

2.1.2. Permanent Magnet Synchronous Generator Modeling

To design the proposed strategy, the PMSG model in dq–frame is adopted, expressed as [17,26]:

$$v_{dq} = R_{dq}i_{dq} + L_{dq}\frac{di_{dq}}{dt} + p\omega_m\Im(L_{dq}i_{dq} + \psi_f)\,, \tag{6}$$

$$J\frac{d\omega_m}{dt} = T_m - T_{em} - f_{fv}\omega_m\,, \tag{7}$$

$$T_{em} = \frac{3}{2}p\psi_{dq}\Im i_{dq} \tag{8}$$

where $i_{dq} = \begin{bmatrix} i_d \\ i_q \end{bmatrix}$ represents the stator current vector, T_{em} denotes the electromagnetic torque, $L_{dq} = \begin{bmatrix} L_d & 0 \\ 0 & L_q \end{bmatrix}$ represents the matrix of the stator induction, f_{fv} represents the viscous coefficient, θ_e represents the electrical angular, $v_{dq} = \begin{bmatrix} v_d \\ v_q \end{bmatrix}$ denotes the voltage stator vector, $R_{dq} = \begin{bmatrix} R_S & 0 \\ 0 & R_s \end{bmatrix}$ represents the stator resistance matrix, $\psi_{dq} = \begin{bmatrix} \psi_d \\ \psi_q \end{bmatrix} = \begin{bmatrix} L_d i_d + \psi_f \\ L_q i_q \end{bmatrix}$ is the flux linkages vector, ω_m denotes the PMSG speed, ψ_f are the flux linkages due to the permanent magnets, p is the number of pole-pairs, $\Im = \begin{bmatrix} 0 & -1 \\ 1 & 0 \end{bmatrix}$, and T_m is the mechanical torque output of the turbine.

2.2. Verification of the Proposed Control's Applicability

As mentioned previously, the design of the proposed fuzzy supervisory passivity-based speed control (FS-PBSC) needs several steps to be verified. Firstly, it is required to demonstrate the passivity property of the PMSG model such that the proposed method can be applied. Secondly, the PMSG needs to decompose into two passive sub-systems with negative feedback. Finally, the PMSG model's non-dissipative terms are identified to compute a controller with a simple structure. Two steps are distinguished in the investigated candidate process shown in Figure 2. The first step consists of the design of the reference current through the mechanical torque and the desired speed which is the tidal speed, and then the controller law is computed using the developed FS-PBSC strategy.

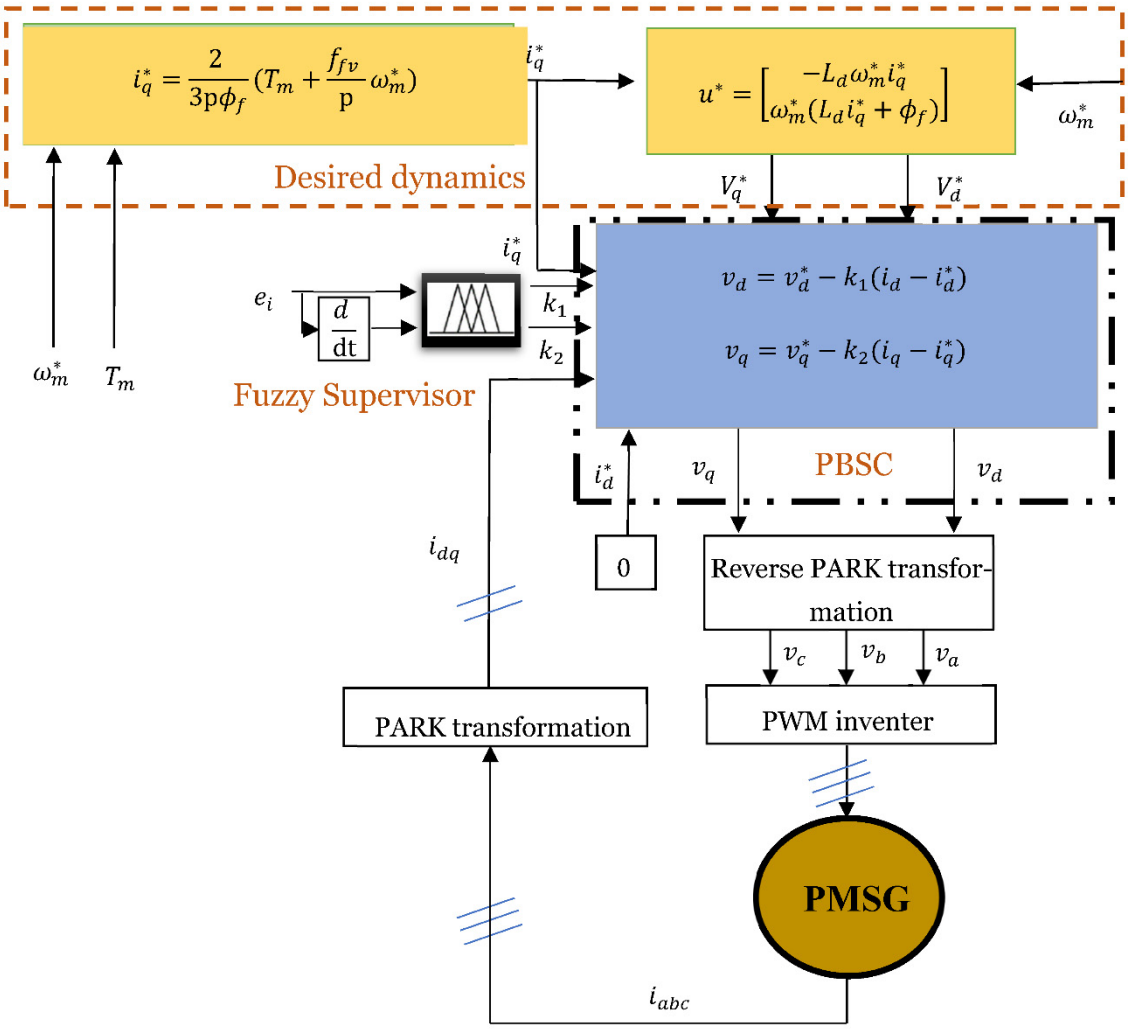

Figure 2. Supervisory energy-based speed controller diagram. Note: * superscript represents the reference values.

2.2.1. PMSG Dq-Model Decomposition into Two Sub-Systems Interconnected with Passive Feedback

The PMSG model given by (6)–(8) can be re-arranged as follows:

$$\sum_e : V_e = \begin{bmatrix} v_{dq} \\ -\omega_m \end{bmatrix} \rightarrow Y_e = \begin{bmatrix} i_{dq} \\ T_m \end{bmatrix}, \tag{9}$$

$$\sum_m : V_m = (-T_e + T_m) \rightarrow Y_m = -\omega_m = \frac{(-T_e + T_m)}{Js + f_{fv}}. \tag{10}$$

The lemma 1 is formulated based on the above (9) and (10), as expressed below:

Lemma 1. *The model (6)–(8) is decomposable into two sub-systems interconnected with passive feedback, i.e., electrical dynamic* $\sum_e$ *and mechanical dynamic* $\sum_m$ *based on the above conditions.*

Proof. From $\sum_e$, the total energy H_e is given below:

$$H_e = \frac{1}{2} i_{dq}^T L_{dq} i_{dq} + \psi_{dq}^T i_{dq}. \tag{11}$$

Time derivative along (6) of H_e, gives:

$$\dot{H}_e = -i_{dq}^T R_{dq} i_{dq} + Y_e^T V_e + \frac{d}{dt}\left(\psi_{dq}^T i_{dq}\right). \tag{12}$$

Integrating Equation (12) along $\begin{bmatrix} 0 & T_e \end{bmatrix}$, yields:

$$\underbrace{H_e(T_e) - H_e(0)}_{\substack{Stored \\ Energy}} = \underbrace{-\int_0^{T_e} i_{dq}^T R_{dq} i_{dq} d\tau}_{\substack{Dissipated \\ Energy}} + \underbrace{\int_0^{T_e} Y_e^T V_e d\tau + \left[\psi_{dq}^T i_{dq}\right]_0^{T_e}}_{\substack{Supplied \\ Energy}} \tag{13}$$

where $H_e(0)$ denotes the initial stored energy and $H_e(T_e) \geq 0$. Integrating Equation (13), yields the following dissipation inequality:

$$\int_0^{T_e} Y_e^T V_e d\tau \geq \lambda_{min}\left\{R_{dq}\right\} \int_0^{T_e} \|i_{dq}\|^2 d\tau - (H_e(0) + \left[\psi_{dq}^T i_{dq}\right]_0^{T_e}) \tag{14}$$

where $\|.\|$ denotes the Euclidian vector norm.

Then, it is deduced from Equation (14) that $\sum_e$ is passive. Thus, $\mathrm{F}_m(s)$ is given as below:

$$\mathrm{F}_m(s) = \frac{\mathrm{Y}_m(s)}{\mathrm{V}_m(s)} = \frac{1}{\mathrm{J}s + f_{fv}} \tag{15}$$

Since $\mathrm{F}_m(s)$ is strictly positive, the mechanical dynamic $\sum_m$ is passive. Then, the PMSG model is decomposable into $\sum_e$ and $\sum_m$. □

2.2.2. PMSG Passivity Property

Lemma 2. *The model (6)–(8) is passive, when* $Y = \left[v_{dq}^T,\ T_e\right]^T$ *and* $X = \left[i_{dq}^T,\ \omega_m\right]^T$ *are chosen as the PMSG outputs and inputs, respectively.*

Proof. First, the PMSG Hamiltonian H_m is defined as:

$$H_m\left(\ i_{dq}, \omega_m\right) = \underbrace{\frac{1}{2} i_{dq}^T L_{dq} i_{dq} + \psi_{dq}^T i_{dq}}_{\substack{Electrical \\ Energy}} + \underbrace{\frac{1}{2} J \omega_m^2}_{\substack{Mecanical \\ Energy}} \tag{16}$$

The derivative along (6)–(8) of H_m, gives:

$$\frac{dH_m\left(\ i_{\alpha\beta}, \omega_m\right)}{dt} = -\frac{d\left(i_{\alpha\beta}^T R\ i_{dq}\right)}{dt} + y^T \nu + \frac{d}{dt}\left(\psi_{dq}^T i_{dq}\right) \tag{17}$$

where $R = \mathrm{diag}\left\{R_{dq}, f_{fv}\right\}$. Integrating (17) along [0 T_m], gives:

$$\underbrace{H_m(T_m) - H_m(0)}_{\substack{Stored \\ Energy}} = \underbrace{-\int_0^{T_m} i_{dq}^T R\ i_{dq}\ d\tau}_{\substack{Dissipated \\ Energy}} + \underbrace{\int_0^{T_m} y^T \nu\ d\tau + [\psi_{dq}^T i_{dq}]_0^{T_m}}_{\substack{Supplied \\ Energy}} \tag{18}$$

where $H_m(0)$ is the stored initial energy and $H_m(T_m) \geq 0$. Integrating (18), yields:

$$\int_0^{T_m} y^T \nu\ d\tau \geq \lambda_{\min}\{R\} \int_0^{T_m} \|i_{dq}\|^2 d\tau - \left(H_m(0) + [\psi_{dq}^T i_{dq}]_0^{T_m}\right) \tag{19}$$

Then, relationship M is passive, which is the same for the PMSG. □

2.2.3. Workless Forces Identification

From the model (6)–(8), the following compact form can be deduced:

$$D\frac{di_{dq}}{dt} + WX + RX = Mv_{dq} + \Gamma \tag{20}$$

where $D = \text{diag}\left\{L_{dq}, J\right\}$, $M = [I_2, 0_{1\times 2}]^T$, $W = \left[\frac{d}{dt}\psi_{dq}^T\omega_m, -i_{dq}\frac{d}{dt}\psi_{dq}\right]^T$, and $\Gamma = [0_{2\times 1}, -T_m]^T$. Based on the PMSG model (20) and the passivity property, the "workless forces" are deduced as given below [27,28]:

$$F = \begin{bmatrix} 0_{2\times 2} & \frac{d}{dt}\psi_{dq} \\ -\frac{d}{dt}\psi_{dq}^T & 0_{1\times 1} \end{bmatrix} \tag{21}$$

As F satisfies:

$$F = -F^T \tag{22}$$

Remark 1. *From Section 2.2, the necessary conditions to apply the PBSC on the PMSG as mentioned in Section 3 have been analytically verified and satisfied.*

2.3. Proposed Passivity-Based Speed-Control Design

In order to design the control strategy, based on the passivity concept, the state-space model of the PMSG is written in the following form:

$$\mathcal{L}\dot{X} = \mathcal{J}(u)X - \mathcal{R}X + \mathcal{B}u + \xi \tag{23}$$

where $\mathcal{L} = \begin{bmatrix} L_d & 0 & 0 \\ 0 & L_q & 0 \\ 0 & 0 & \frac{2J}{3p^2} \end{bmatrix}$ is a constant symmetric positive definite matrix, $\mathcal{R} = \begin{bmatrix} R_s & 0 & 0 \\ 0 & R_s & 0 \\ 0 & 0 & \frac{2\,f_{fv}}{3p^2} \end{bmatrix}$ is the losses matrix, $\mathcal{J}(u) = \begin{bmatrix} 0 & L_d\omega_m & 0 \\ -L_d\omega_m & 0 & -\phi_f \\ 0 & \phi_f & 0 \end{bmatrix}$ is a skew symmetric matrix, $\xi = \begin{bmatrix} 0 \\ 0 \\ -\frac{2\,T_m}{3\text{p}} \end{bmatrix}$ is the disturbance vector, $\mathcal{B} = \begin{bmatrix} 1 & 0 \\ 0 & 1 \\ 0 & 0 \end{bmatrix}$, and u denotes the input-matrix which is the controller law defined as:

$$u = \begin{bmatrix} v_d \\ v_q \end{bmatrix} \tag{24}$$

To guarantee that the defined state model (23) of the PMSG, is the system that can be controlled by passivity, the matrices $\mathcal{J}(u)$ and $\mathcal{R}$ must satisfy the conditions $\mathcal{J}^T(u) = -\mathcal{J}(u)$ and $\mathcal{R}^T = \mathcal{R}$.

By considering that the aforementioned conditions are satisfied, the reference voltage vector $u^* = \begin{bmatrix} v_d^* & v_q^* \end{bmatrix}^T$ is considered as the desired input and $X^* = \begin{bmatrix} i_q^* & i_q^* & \omega_m^* \end{bmatrix}^T$ is the desired state variable. This yields the desired dynamic state model of the PMSG given below:

$$\mathcal{L}\dot{X^*} = \mathcal{J}(\text{u})X^* - \mathcal{R}X^* + \mathcal{B}\text{u}^* + \xi, \tag{25}$$

The desired control input u^* is computed by the proposed strategy, using the previous simplified model (25).

The differences between u and u^*, X and X^* representing the voltage tracking error and the state variables tracking error, respectively, are described by:

$$e_u = \begin{bmatrix} e_{ud} \\ e_{uq} \end{bmatrix} = u - u^* , \tag{26}$$

$$e = \begin{bmatrix} e_d \\ e_q \end{bmatrix} = X - X^* \tag{27}$$

Substituting Equation (23) in Equation (25), yields

$$\mathcal{L}\dot{e} = [\mathcal{J}(u) - \mathcal{J}(u^*)]X - \mathcal{R}e + \mathcal{B}e_u + \mathcal{J}(u^*)e \tag{28}$$

Principally, it is a linear control for the nonlinear dynamical of the PMSG. Using the Taylor series, $\mathcal{J}(u)$ can be linearized as follows:

$$\mathcal{J}(u) = \mathcal{J}(u^*) + \left.\frac{d\mathcal{J}(u)}{du}\right|_{u^*} e_u \tag{29}$$

where $\left.\frac{d\mathcal{J}(u)}{du}\right|_{u^*} e_u = 0$ since $\mathcal{J}(u)$ is a constant matrix.

Substituting Equation (29) into Equation (28), yields

$$\mathcal{L}\dot{e} = -\mathcal{R}e + \mathcal{B}e_u + \mathcal{J}(u^*)e \tag{30}$$

The aim is to ensure the convergence to zero of the error vectors e_u and the stability property of Equation (30), by finding the desired input u^*. Using the Lyapunov theory, the following energy function of the closed-loop system is defined by:

$$V(\mathrm{e}) = 0.5\mathrm{e}^T\mathcal{L}\mathrm{e} \tag{31}$$

Taking the time derivative of $V(\mathrm{e})$ along trajectory (30), gives:

$$\dot{V}(\mathrm{e}) = -\mathrm{e}^T\mathcal{R}\mathrm{e} + \mathrm{e}^T\mathcal{B}e_u \tag{32}$$

The term $\mathrm{e}^T\mathcal{J}(u^*)e$ does not appear on the right-side of (32), due to $\mathrm{e}^T\mathcal{J}(u^*)$ which is nonsymmetrical. By considering $e_u = -k_e\mathcal{B}^Te$, Equation (32) becomes:

$$\dot{V}(\mathrm{e}) = -\mathrm{e}^T\left(\mathcal{R} + \mathcal{B}k_e\mathcal{B}^T\right)e \tag{33}$$

where $k_e = \begin{bmatrix} k_1 & 0 \\ 0 & k_2 \end{bmatrix}$ with $k_1 > 0$ and $k_2 > 0$.

Taking $\left(\mathcal{R} + \mathcal{B}k_e\mathcal{B}^T\right) \geq 0$ with the aim to make the energy function $\dot{V}(\mathrm{e})$ negatively defined, which guarantees the stability of Equation (30) and assuming that $e_u = u - u^* = -k_e\mathcal{B}^Te$, gives:

$$e_u = -\begin{bmatrix} k_1 & 0 \\ 0 & k_2 \end{bmatrix}\begin{bmatrix} 1 & 0 & 0 \\ 0 & 1 & 0 \end{bmatrix}\begin{bmatrix} i_d - i_d^* \\ i_q - i_q^* \\ \omega_m - \omega_m^* \end{bmatrix} = -\begin{bmatrix} k_1\left(i_d - i_d^*\right) \\ k_2\left(i_q - i_q^*\right) \end{bmatrix} \tag{34}$$

Then, the control signals $u = \begin{bmatrix} v_d & v_q \end{bmatrix}^T$ are deduced, which ensure the convergence of the voltage tracking error e_u. Then, the control voltage vector is given by:

$$u = \begin{bmatrix} v_d \\ v_q \end{bmatrix} = \begin{bmatrix} v_d^* - k_1\left(i_d - i_d^*\right) \\ v_q^* - k_2\left(i_q - i_q^*\right) \end{bmatrix} \tag{35}$$

The voltage controller u, consists of two parts: The desired reference vector u^* and the damping term to make the closed-loop system strictly passive. However, it is well known that fixed gains are very sensitive when the system is exposed to parameter uncertainties and external disturbances. As shown in Figure 3, to overcome the problem due to fixed gains and to compute an optimal controller, a fuzzy controller is introduced as a supervisor to compute the damping gains k_1 and k_2 to overcome the problem caused by parameter uncertainties, which makes the proposed PBSC intelligent. The current error $e_i = \left(i_d - i_d^*\right)$ and its derivative are taken as the inputs of the fuzzy supervisor. The selected fuzzy control design process consists of fuzzification of the inputs, formulation of the rules, and finally defuzzification of the output. Based on types including triangular and trapezoidal shapes, the membership functions are chosen to be symmetrical and uniformly distributed as given in Figure 4. The Lee and Yubazaki [29,30] technique of dividing these functions is utilized, which consists of many membership functions exchanging the same parameter. The significant reduction of the parameter numbers of the membership functions is the advantage of this method. The inputs-outputs linguistic variables corresponding to the fuzzy block are tabulated in Table 1, which are defined as: Positive Small (PS), Positive Big (PB), Zero (Z), Negative Big (NB), and Negative Small (NS). A Max-Min fuzzy inference is used for the decision-making where the center of gravity defuzzification method is used to calculate the crisp outputs [23].

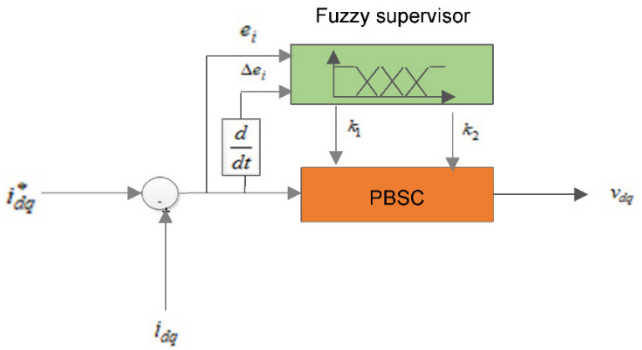

Figure 3. Damping gains with the fuzzy supervisor.

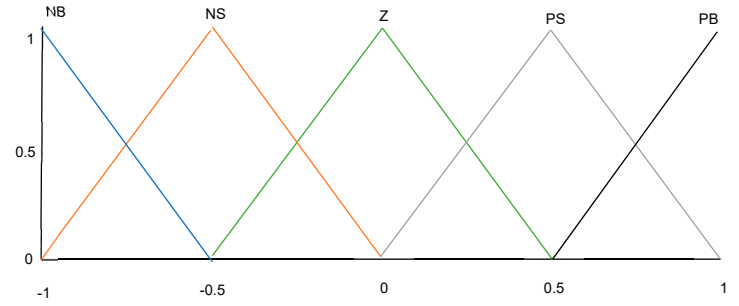

(**a**)

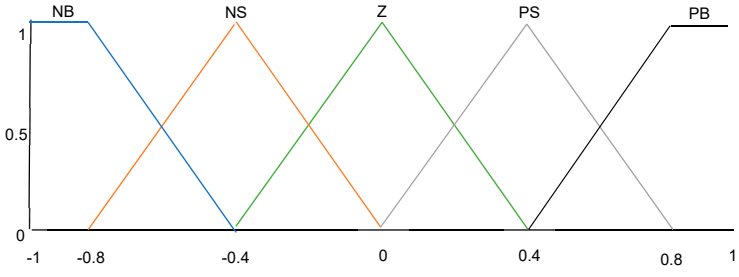

(**b**)

Figure 4. The fuzzy supervisor designs. (**a**) Inputs function; (**b**) outputs function.

Table 1. Fuzzy logic rules.

ε_i \ $\Delta\varepsilon_i$	**NB**	**NS**	**Z**	**PS**	**PB**
NB	NB	NB	NS	NS	Z
NS	NB	NB	NS	Z	PS
Z	NS	NS	Z	PS	PS
PS	NS	Z	PS	PB	PB
PB	Z	PS	PS	PB	PB

Remark 2. *As shown in Figure 2, the proposed method ensures the current and speed tracking errors convergence. The damping term "$k_e\mathcal{B}^T e$" ensures convergence of the voltage tracking error "e_u" (Equation (34)). The condition $\left(\mathcal{R} + \mathcal{B}k_e\mathcal{B}^T\right) \geq 0$ ensures a negative time derivative of the function $\dot{V}(e)$ (Equation (33)), thus the convergence of the voltage tracking error "e_u", and then, the equality between the voltage u which is the controller law and the desired u^* (Equation (35)). Therefore, the convergence of the voltage tracking error "u-u^*" should be ensured.*

2.4. Desired Voltage and Desired Current Computation

In order to design the control strategy, based on the passivity concept, the state-space model of the PMSG is written in the following form [15]:

The voltage reference u^* and the desired stator currents $i^*_{dq} = \begin{bmatrix} i^*_d & i^*_q \end{bmatrix}^T$ are computed from the system equilibrium point ($\dot{X} = 0$) described by Equation (34):

$$\begin{bmatrix} L_d\omega^*_m i^*_q - R_s i^*_d + V^*_d \\ -\omega^*_m\left(L_d i^*_q + \phi_f\right) - R_s i^*_d + V^*_q \\ \phi_f i^*_q - \frac{2}{3\mathrm{p}}\left(T_m + \frac{f_{fv}}{\mathrm{p}}\omega^*_m\right) \end{bmatrix} = \begin{bmatrix} 0 \\ 0 \\ 0 \end{bmatrix} \tag{36}$$

Knowing that the PMSG operates under maximum torque when the desired direct current $i^*_d = 0$. Under this condition, and using Equation (36), it yields

$$u^* = \begin{bmatrix} V^*_d \\ V^*_q \end{bmatrix} = \begin{bmatrix} -L_d\omega^*_m i^*_q \\ \omega^*_m\left(L_d i^*_q + \phi_f\right) \end{bmatrix} \tag{37}$$

$$i^*_q = \frac{2}{3\mathrm{p}\phi_f}\left(T_m + \frac{f_{fv}}{\mathrm{p}}\omega^*_m\right) \tag{38}$$

2.5. Grid-Side Converter (GSC) Proposed Control

To regulate and transmit to the electrical energy produced by the PMSG to the grid through the GSC, a classical method is selected which consists of the PI strategy. As shown in Figure 5, the distributed network PI current controller contains two closed controls, the inner consists of injecting only the active power into the grid by enforcing quadrature current i_{qf} to zero, and the *d*-axis reference current i_{df} is determined by the *DC*-bus voltage controller, while, the *q*-axis current i_{qf} is produced by the reactive power Q_g which is the outer. The GSC mathematical model is expressed as follows [1,19]:

$$\begin{bmatrix} V_d \\ V_q \end{bmatrix} = R_f \begin{bmatrix} i_{df} \\ i_{qf} \end{bmatrix} + \begin{bmatrix} L_f\frac{di_{df}}{dt} - \omega L_f i_{qf} \\ L_f\frac{di_{qf}}{dt} + \omega L_f i_{df} \end{bmatrix} + \begin{bmatrix} V_{gd} \\ V_{gq} \end{bmatrix} \tag{39}$$

where V_{gd} and V_{gq} are the grid voltages, i_{df} and i_{qf} are the grid currents, R_f represents the filter's resistance, L_f represents the filter inductance, ω denotes the network angular

frequency, and V_d and V_q denote the inverter voltages. The DC-link voltage mathematical model is formulated below [1]:

$$C\frac{dV_{dc}}{dt} = \frac{3}{2}\frac{v_{gd}}{V_{dc}}i_{df} + i_{dc} \tag{40}$$

where C is the DC-link capacitance, i_{dc} is the line current, and V_{dc} is the DC-link voltage. The mathematical model of PI current loop controller is formulated as follows:

$$\begin{cases} V_{gd}^{PI} = k_{gp}^{d}\left(i_{df}^{ref} - i_{df}\right) - k_{gi}^{d}\int_0^t\left(i_{df}^{ref} - i_{df}\right)d\tau \\ V_{gq}^{PI} = k_{gp}^{q}\left(i_{qf}^{ref} - i_{qf}\right) - k_{gi}^{q}\int_0^t\left(i_{qf}^{ref} - i_{qf}\right)d\tau \end{cases} \tag{41}$$

where $k_{gp}^{d} > 0$, $k_{gi}^{d} > 0$, $k_{gp}^{q} > 0$, and $k_{gi}^{q} > 0$. The mathematical model of DC-link PI loop is formulated as:

$$i_{qf}^{ref} = k_{dcp}\left(V_{dc\_ref} - V_{dc}\right) - k_{dci}\int_0^t\left(V_{dc\_ref} - V_{dc}\right)d\tau \tag{42}$$

where $k_{dcp} > 0$ and $k_{dci} > 0$. Finally, the mathematical model of the active and reactive powers is formulated as follows below:

$$\begin{cases} P_g = \frac{3}{2}V_{gd}i_{df} \\ Q_g = \frac{3}{2}V_{gd}i_{qf} \end{cases} \tag{43}$$

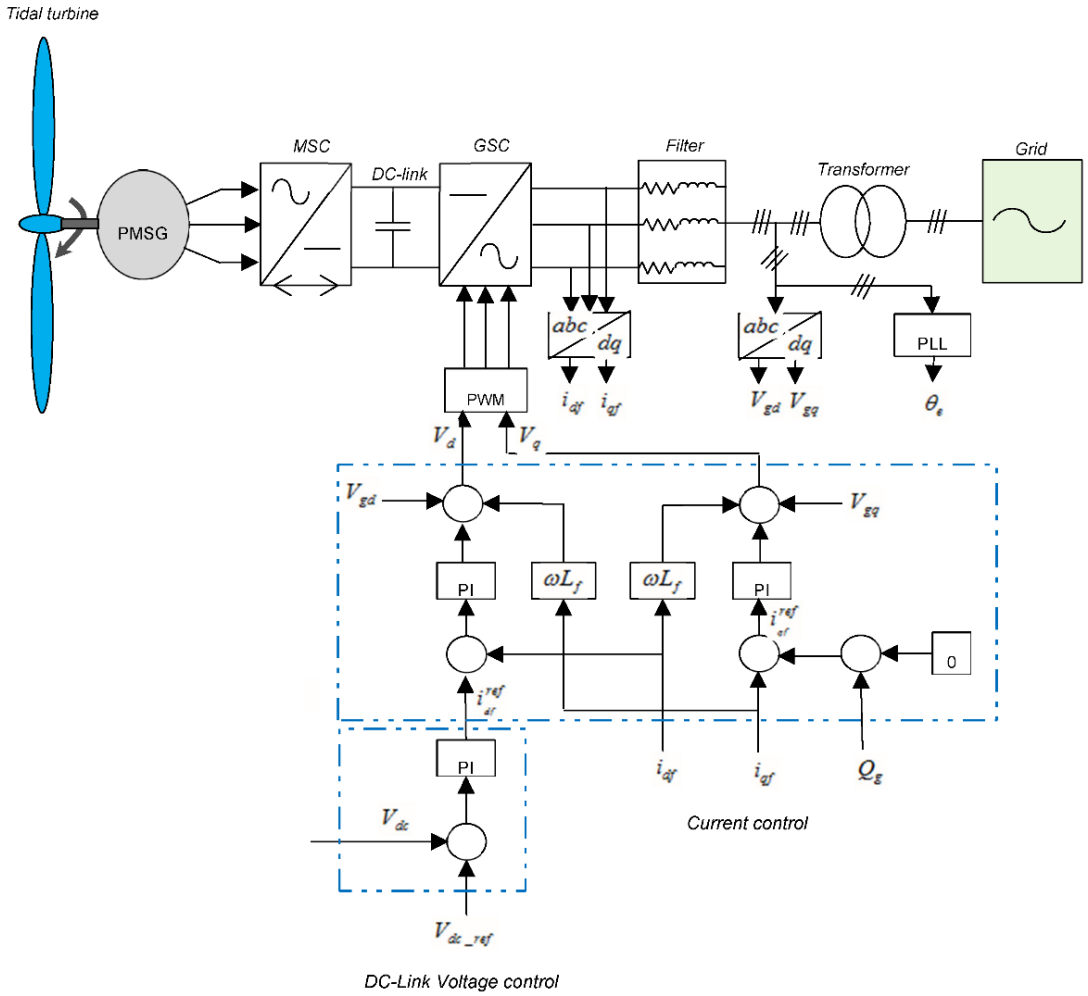

Figure 5. Grid-side control strategy.

3. Simulation and Experimental Results

To demonstrate the effectiveness of the proposed strategy shown in Figure 2, the numerical investigation is performed on the conversion using MATLAB/Simulink and implemented in the processor in the loop (PIL) experiment. The parameter values of the closed-loop are given in Table 2, with 1150 V and zero values chosen as the reference command for V_{dc} and Q_g, respectively. The initial values of the parameters are given as: $[\omega_m(0), i_{dq}(0)] = [0,0,0]$, V_{dc} (0) = 0, and $i_{dqf}(0) = [0,0]$. Using the pole location method, the GSC current PI gains are given as: $k_{gp}^d = k_{gp}^q = 9$ and $k_{gi}^d = k_{gi}^q = 200$. The DC-link PI gains are: $k_{dcp} = 5$ and $k_{dci} = 500$. The investigated strategy is compared with other nonlinear controls to show its superiority, with the fuzzy passivity-based linear feedback current control (FPBLFC) proposed in [17], the passivity-based current control (PBCC) proposed in [18], the high-order sliding mode control (HSMC) [7], and the passivity-based fuzzy high order sliding mode (PBC-HSMC) [31]. The proposed method is tested under two scenarios. First, the proposed controller is tested with initial parameter values of the PMSG and compared with the benchmark controls. The second task deals with the robustness analysis of this proposed method due to parameter changes.

Table 2. System parameters.

PMSG Parameter	Value
Tidal density (ρ)	1024 kg/m^2
Tidal turbine radius (R)	10 m
Stator inductance (L_{dq})	0.3 mH
Stator resistance (R_s)	0.006 Ω
Stator inductance (L_{dq})	0.3 mH
Pole pairs number (p)	48
Flux linkage (φ_f)	1.48 Wb
Total inertia (J)	35,000 kg.m^3
DC-link voltage (V_{dc})	1150 V
DC-link capacitor (C)	2.9 F
Grid-filter resistance (R_f)	0.3 pu
Grid-filter inductance (L_f)	0.3 pu

3.1. Performance Analysis under Fixed Parameters

Figure 6 depicts the profile of the tidal speed imposed to the conversion system with a fast-sudden variation between 4 and 10 m/s to test the stability of the designed control. Figure 7 depicts the DC voltage response due to the proposed FS-PBSC, FPBLFC, PBCC, PBC-HSMC, and HSMC controls. Given the shown responses and Table 3, a transient undershoot of −0.002 and overshoot of +0.002 are observed with the proposed FS-PBSC, a transient undershoot of −0.006 and overshoot of +0.006 are observed with the PBC-HSMC, a transient undershoot of −0.02, −0.03, and −0.2 are observed with the FPBLFC, PBCC, and HSMC methods, respectively and transient overshoot of +0.02, +0.03, and +0.2. From the tracing response of the DC-bus given by Figures 7 and 8, it can be seen that the DC voltage error (ε (V_{dc})) is extremely reduced in the case of the proposed FS-PBSC, which shows that the conversion system offers a reliable and efficient electrical energy to the grid with the proposed strategy. Figures 9 and 10 illustrate the tracking error (ε (Q_g)) of Q_g due to the investigated FS-PBSC, PBC-HSMC, FPBLFC, PBCC, and HSMC where the transient undershoot and overshoot of -1.5×10^{-5}, -1.5×10^{-5}, -4×10^{-5}, -5×10^{-5}, -7×10^{-5} and $+1.5 \times 10^{-5}$, $+1.5 \times 10^{-5}$, $+4 \times 10^{-5}$, $+5 \times 10^{-5}$, $+7 \times 10^{-5}$ are observed, respectively. However, the lowest undershoot and overshoot are illustrated by the proposed FS-PBSC according to Table 3. Moreover, the lowest steady-state error and better convergence criterion is shown by the proposed FS-PBSC and PBC-HSMC (0.3×10^{-3} s) over the FPBLFC (1×10^{-3} s), PBCC (1.2×10^{-3} s), and HSMC (2×10^{-3} s) as depicted in Table 4, which shows also that the proposed FS-PBSC ensures fast convergence, high efficiency, and the lowest tracking errors in comparison to the tested benchmark nonlinear strategies,

as well as offers a stable electrical power to the grid. Thus, from the previous results shown in Figures 7–10, the proposed method validates the objective mentioned in the introduction part which is regulation of the DC-link voltage (Figures 7 and 8) and reactive power (Figures 9 and 10) at their pre-fault values to guarantee efficient, secure, and reliable electricity, which are indeed any possible disturbances related to the MSC such as sudden changes in tidal velocity and PMSG nonlinear properties.

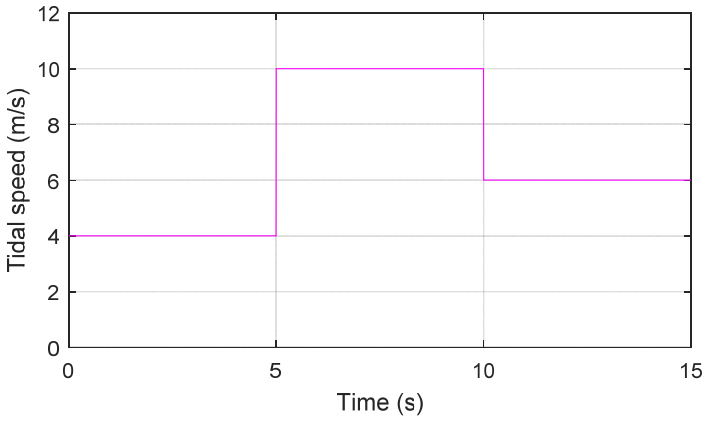

Figure 6. Tidal velocity.

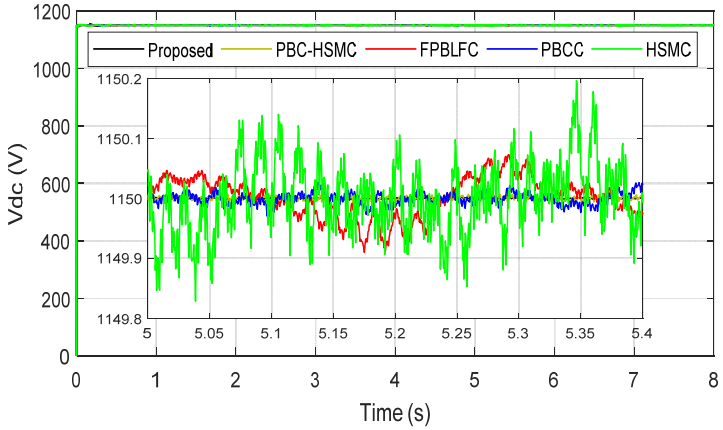

Figure 7. DC-link voltage response.

Table 3. Initial parameter results of the control strategies.

Control	Proposed	FPBLFC	PBCC	HSMC	PBC-HSMC
Variation	R_s and J	R_s and J	R_s and J	R_s and J	R_s and J
V_{dc} (V)	±1150.002	±1150.02	±1150.03	±1150.2	±1150.006
Q_g (MW)	$\pm 1.5 \times 10^{-5}$	$\pm 4 \times 10^{-5}$	$\pm 5 \times 10^{-5}$	$\pm 7 \times 10^{-5}$	$\pm 1.5 \times 10^{-5}$
ε (V_{dc})	±0.002	±0.02	±0.03	±0.2	±0.006
ε (Q_g)	±0.000015	±0.00004	±0.00004	±0.00007	±0.000015

Table 4. Control strategies performances comparison.

Controls	Proposed	FPBLFC	PBCC	HSMC	PBC-HSMC
Response speed	Extremely fast (0.8×10^{-3} s)	Very fast (1×10^{-3} s)	Fast (1.2×10^{-3} s)	Slow (2×10^{-3} s)	Extremely fast (0.8×10^{-3} s)
Stability	highly stable (fluctuations free)	Very stable (fluctuations free)	Stable (with fluctuations)	Poor stability (with fluctuations)	highly stable (fluctuations free)
Robustness	High robustness	Very Robust	Robust	Not robust	High robustness
Complexity	Extremely Low (with Zero Fixed Gains)	Low (with three Fixed Gains)	Low (with five Fixed gains)	Low (with six Fixed Gains)	Very Low (with Zero Fixed Gains)
Performance	Higher	Very Good	Good	low	Higher

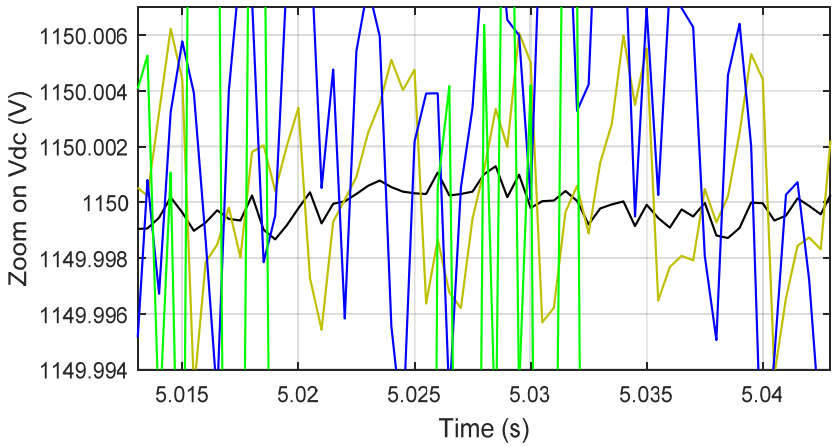

Figure 8. Zoom on DC-link voltage response.

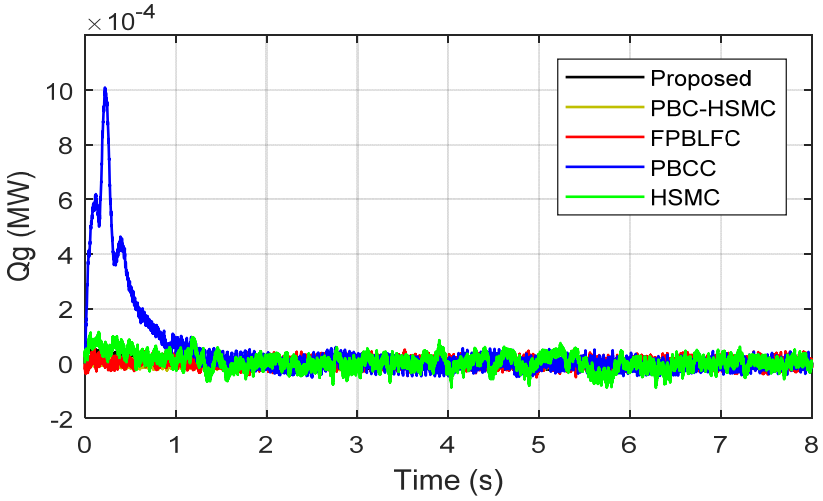

Figure 9. Reactive power response.

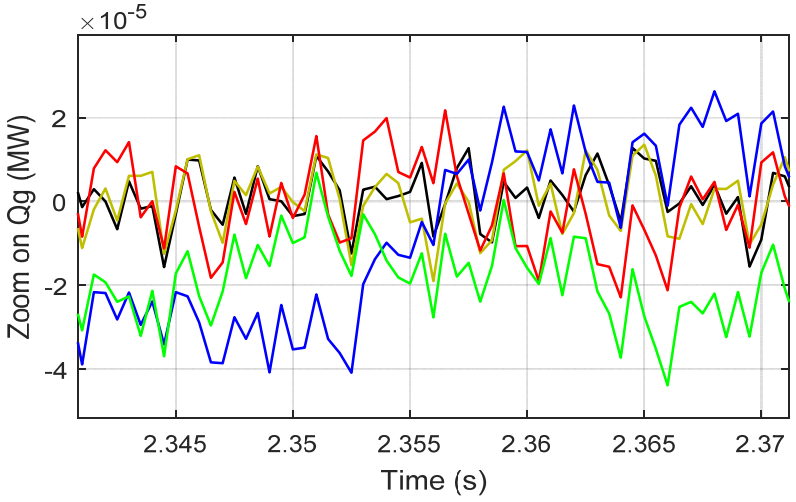

Figure 10. Zoom on reactive power.

3.2. Robustness Analysis

In the present sub-section, the system is supposed to work under parameter disturbances. Thus, a change of +50% in R_s, a change of +100% in J, and a simultaneous change of +50% in R_s and +100% in J are imposed on the closed-loop, respectively. Figure 11

shows the DC-link voltage response due to the proposed candidate in the case of +50% in R_s, where the same voltage error ε (V_{dc}) response and tracking error equal to zero are recorded, i.e., ±0.002 according to Table 5 which is the same as in Section 3.1, which shows that the conversion system offers a reliable and efficient electrical energy to the grid with the proposed strategy even under parameter uncertainties. Similarly, the tracking response of Q_g for the diturbances of +50 R_s is observed in Figure 12, i.e., $\pm 2 \times 10^{-5}$ according to Table 5. Figure 13 shows the DC-link voltage response due to the proposed FS-PBSC in the case of variation of +100% in J. Moreover, no changes in the voltage error ε (V_{dc}) response is recorded, i.e., ±0.002 according to Table 4. Figure 14 shows the Q_g response for the disturbances of +100 J, one can see that this disturbance does not influence the dynamic of the system, i.e., $\pm 1.5 \times 10^{-5}$ according to Table 4. Simultaneous change of +50% in R_s and +100% in J have no effect on both V_{dc} and Q_g according to Figures 15 and 16, and the measured values of both V_{dc} and Q_g tabulated in Table 4, which shows also that the proposed FS-PBSC ensures the lowest tracking errors, and offers a stable electrical power into the grid, even under parameter uncertainties. Thus, the previous results shown in Figures 11–16 clearly demonstrate the robustness of the proposed strategy.

Table 5. Robustness comparison of the control strategies.

Control	Proposed			FPBLFC			PBCC			HSMC		
Change	1.5 R_s	1.5 J	1.5 R_s and 1.5	1.5 R_s	1.5 J	1.5 R_s and 1.5 J	1.5 R_s	1.5 J	1.5 R_s and 1.5 J	1.5 R_s	1.5 J	1.5 R_s and 1.5 J
V_{dc} (V)	±1150.002	±1150.002	±1150.002	±1150.06	±1150.04	±1150.04	±1150.08	±1150.07	±1150.08	±1150.9	±1150.9	±1151
Q_g (MW)	$\pm 2 \times 10^{-5}$	$\pm 1.5 \times 10^{-5}$	$\pm 1.5 \times 10^{-5}$	$\pm 5 \times 10^{-5}$	$\pm 4.5 \times 10^{-5}$	$\pm 5 \times 10^{-5}$	$\pm 6 \times 10^{-5}$	$\pm 5.5 \times 10^{-5}$	$\pm 6 \times 10^{-5}$	$\pm 7.5 \times 10^{-5}$	$\pm 8 \times 10^{-5}$	$\pm 8 \times 10^{-5}$
ε (V_{dc})	± 0.002	± 0.002	±0.002	± 0.06	±0.04	±0.04	±0.08	±0.07	±0.08	±0.9	±0.9	±0.95
ε (Q_g)	±0.00002	±0.000015	±0.000015	±0.000055	±0.00005	±0.00005	±0.00006	±0.00005	±0.00006	±0.0009	±0.0001	±0.0001

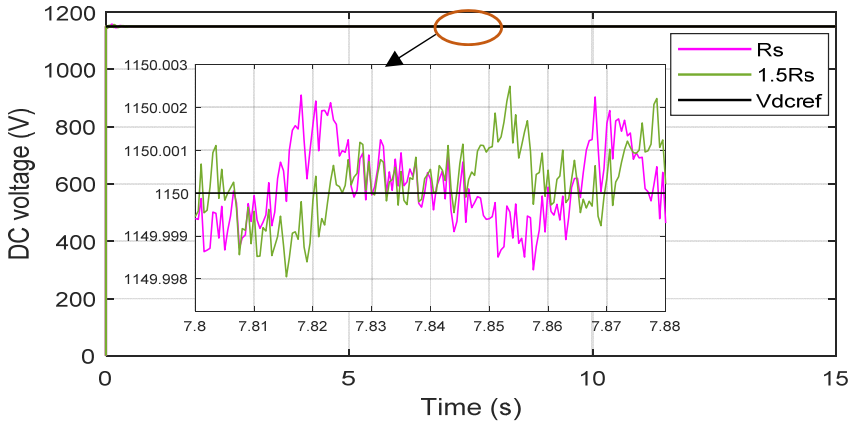

Figure 11. DC-link voltage response of +50% of Rs.

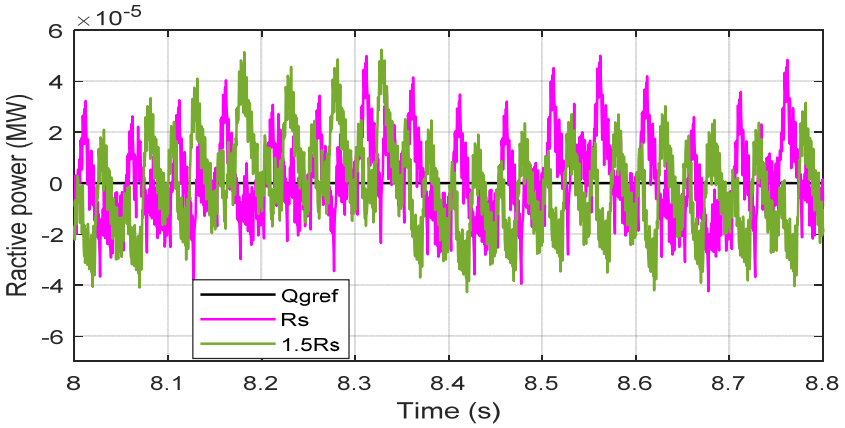

Figure 12. Zoom on reactive power response of +50% of Rs.

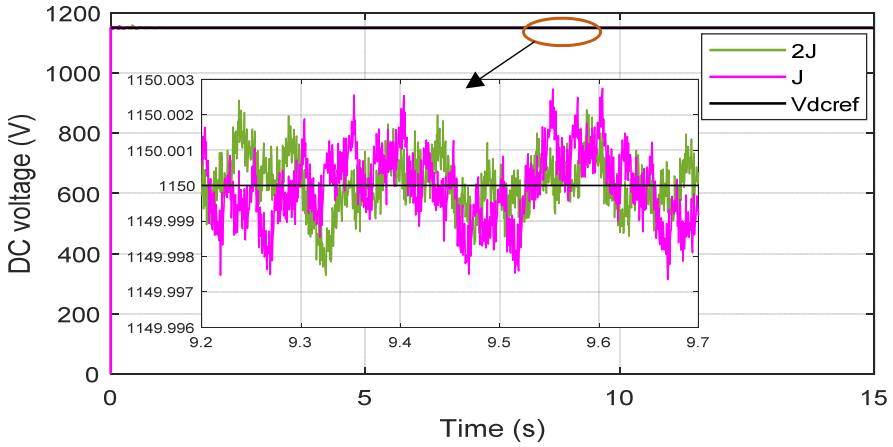

Figure 13. DC-link voltage response of +100% of J.

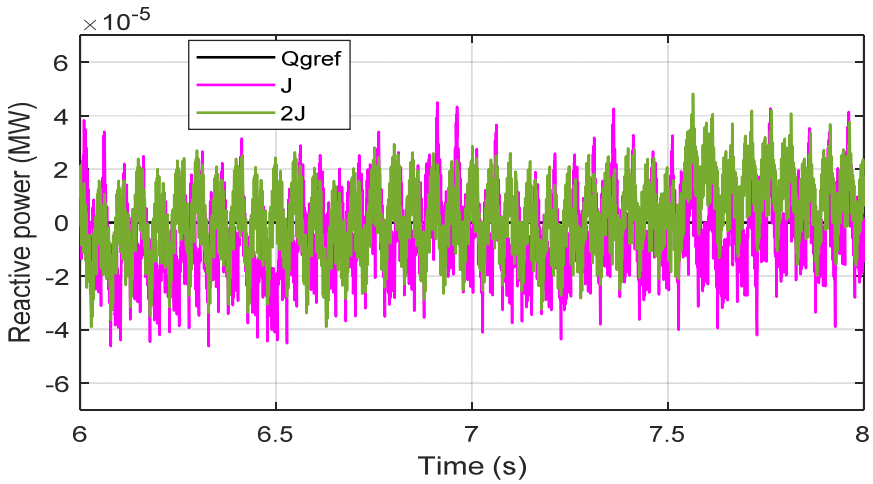

Figure 14. Zoom on reactive power response of +100% of J.

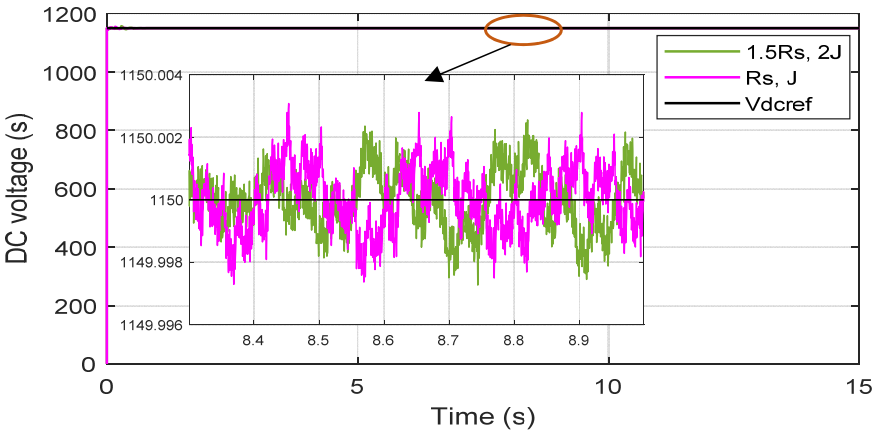

Figure 15. DC-link response of +50% of R_s and +100% of J.

A comparative analysis of the proposed FS-PBSC with the other control strategies is performed in Tables 4 and 5. From Table 4, PBC-HSMC exhibits an ε (V_{dc}) tracking error of ±0.006, PBLFC exhibits an ε (V_{dc}) tracking error of ±0.02, PBCC exhibits ±0.03, and HSMC shows a tracking error of ±0.2. From the presented results, the proposed strategy clearly offers a constant voltage error V_{dc} and superior tracking error speed as compared to the other candidates, which are sensitive to the imposed disturbances of R_s and J. Table 5 depicts the Q_g response for all the tested controls. From the present

results, the proposed FS-PBSC and PBC-HSMC exhibit a reduced tracking error under variations than that exhibited by FPBLFC ($\pm 5 \times 10^{-5}$), PBCC ($\pm 6 \times 10^{-5}$), and HSMC ($\pm 1 \times 10^{-4}$), according to Table 5. Furthermore, the proposed FS-PBSC clearly offers superior speed tracking error ε (Q_g) even under disturbances as compared to the other candidates, which are more affected by the disturbances of R_s and J, as shown in Table 4. Thus, from the present test and tables, the proposed candidate offers high robustness, fast speed convergence, and high efficiency over the other benchmark nonlinear strategies. This validates the theoretical results of Section 2. Figure 17 shows the power coefficient response which is fixed at its reference value (C_{pmax} = 0.46), which shows that the tidal turbine extracts the maximum power from the marine current and thus, validates the first objective mentioned in the introduction, which is to extract the maximum marine current power through controlling the rotational of the PMSG. Moreover, from Figure 18 which shows the grid injected voltage, it is observed that the grid voltage is in a perfect sinusoidal form, which shows that the closed-loop integrates efficient electrical power into the grid. As mentioned in the introduction, the DC-link overvoltage control, reactive power support, efficiency of the power electronics, and ride-through fault capability are the important requirements of the conversion system for reliable and efficient electrical energy, which are validated by the presented results.

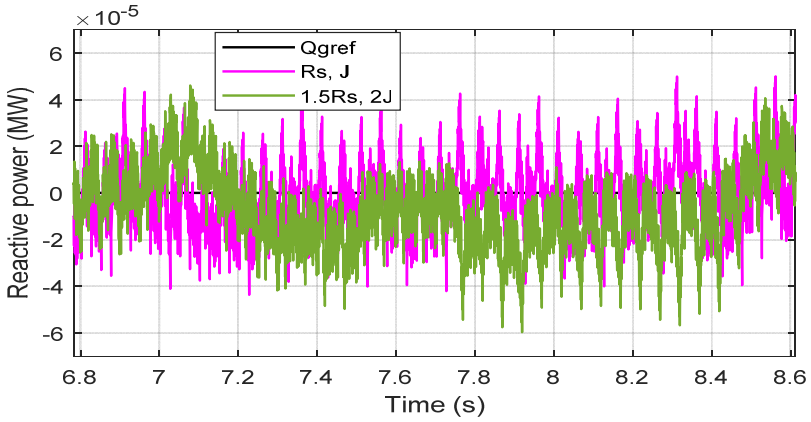

Figure 16. Zoom on reactive power response of +50% of R_s and +100% of J.

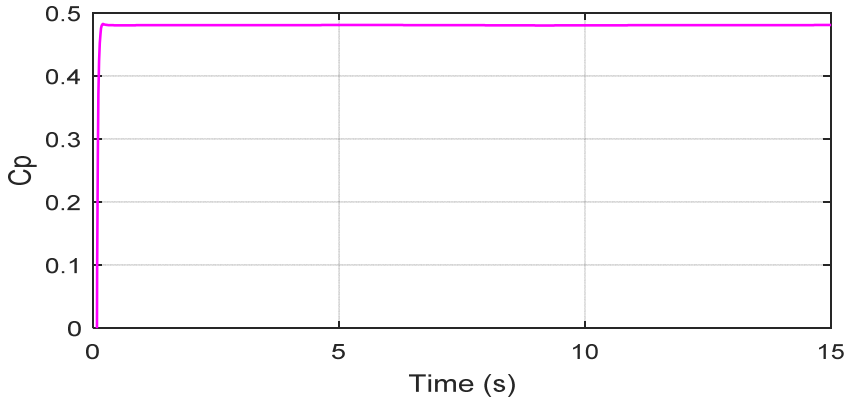

Figure 17. Power coefficient with (C_{pmax} = 0.46).

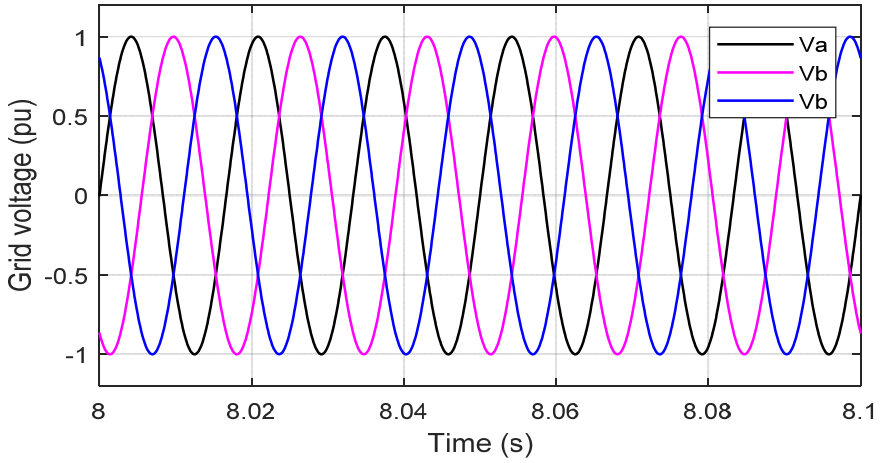

Figure 18. Grid Voltage.

3.3. Processor in the Loop (PIL) Experimental Validation

The processor in the loop experimentation is a powerful tool which is utilized for validating the control system on a hardware processor, while the system plant is a software model. Thus, the control algorithm is tested in real time. More details on the processor in the loop experimentation are reported in [32–34]. More importantly, the controller validated using PIL testing is equally efficient as when it is tested in a hardware plant [32]. Thus, inspired by the above work, the proposed control schemes are tested using a PIL experiment. A photograph of the experimental test platform to validate the proposed technique is shown in Figure 19, which is composed of the computer and the DSP card. Figure 20 shows the block diagram of the proposed control PIL test setups, as shown, in the PIL experiment, the DSP control card is physically integrated with the PMSG-based marine current conversion system model running in the Simulink environment. The control board is made up of a TMS320F379D dual-core processor that was programmed using the Simulink environment's fast prototyping method. Simulink is used to create discrete versions of the described controllers, and the output or hex file is programmed into the processor's random-access memory (RAM). The closed-loop in the PIL experiment is not physical, but rather a Simulink environment, with the controller operating in real time. Using a high-speed serial interface, data are transmitted between the DSP control card and the software model. Figure 21 shows the marine current profile used for the conversion system in the PIL testing. Figure 22 shows the experimental response of the torque collected using the PIL method. It is clearly shown that even in real-time testing, the proposed control forces the PMSG to work at its optimal torque, which further validates the theoretical part of Section 2.3. Figure 23 shows the active power's experimental response which tracks the torque response. This further validates Equation (2) and confirms that the conversion system extracts the maximum tidal power. Figures 24 and 25 show the experimental DC-link voltage response, which is regulated at its reference value of 1150 V. This further validates the simulation results, the objectives of the paper mentioned in the introduction, even in real-time testing, and confirms that it delivers a high voltage quality to the grid shown in Figure 18. Figure 26 shows the reactive power which is fixed at its zero-reference value. From the experimental results, it is very obvious that the proposed strategy is applicable practically and further validates that the proposed control provides high efficiency even in real-time testing.

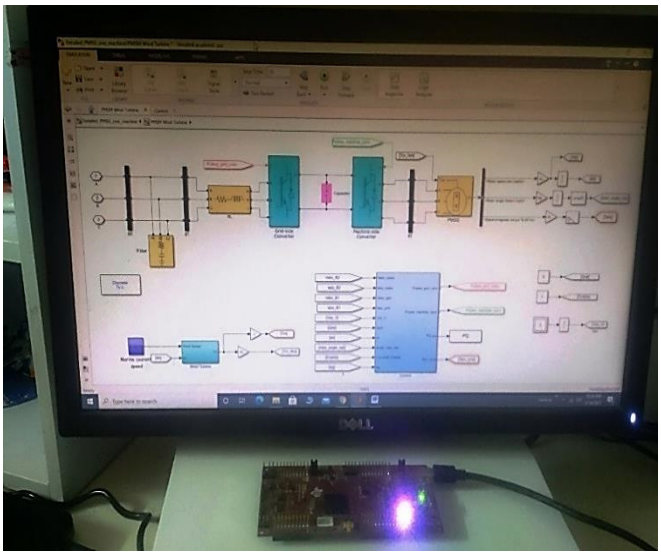

Figure 19. Experimental DSP board.

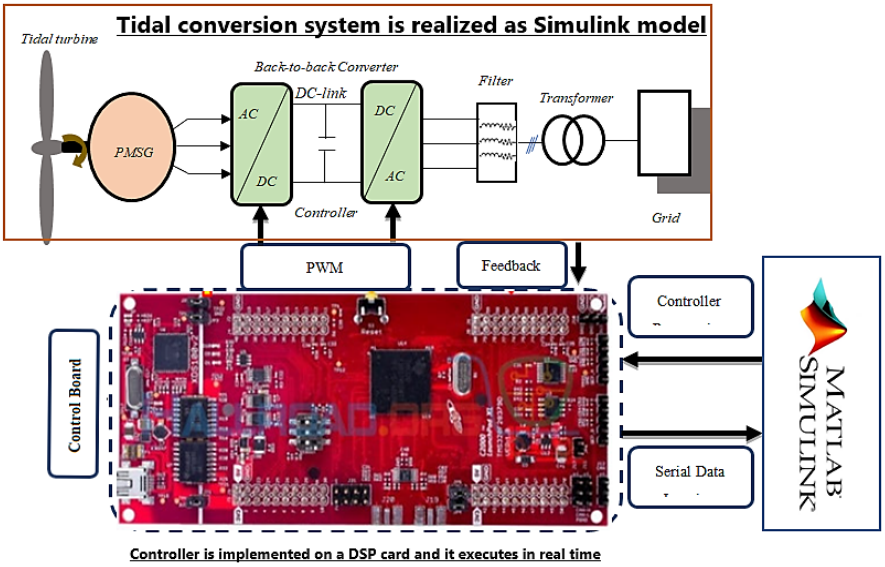

Figure 20. Experimental step.

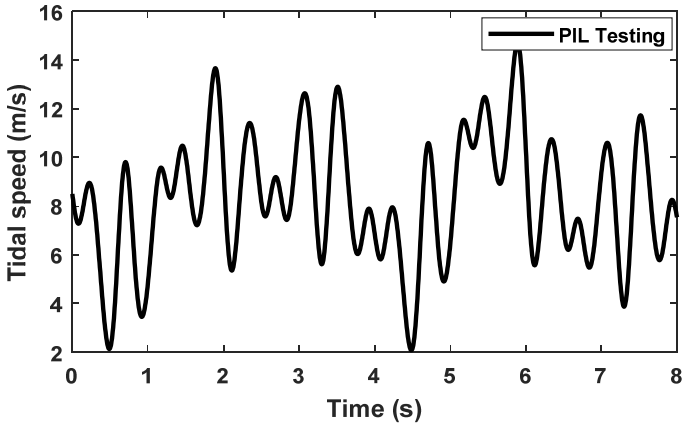

Figure 21. Random profile of marine currents.

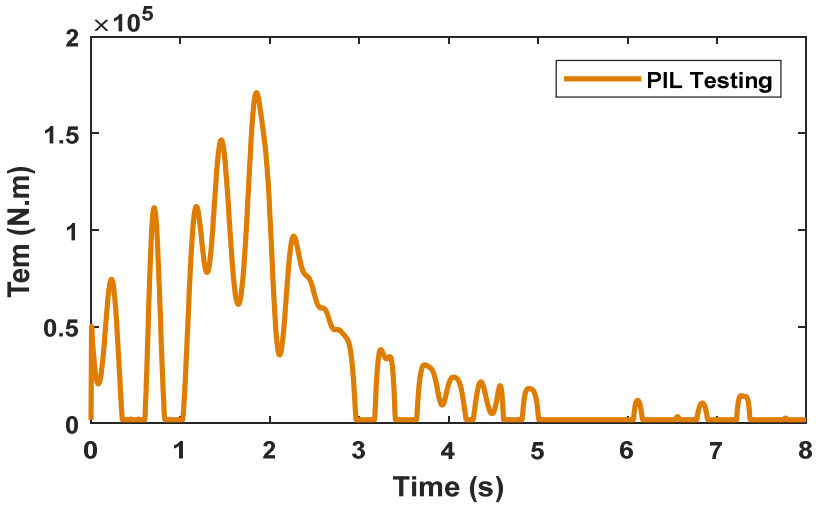

Figure 22. Experimental electromagnetic torque.

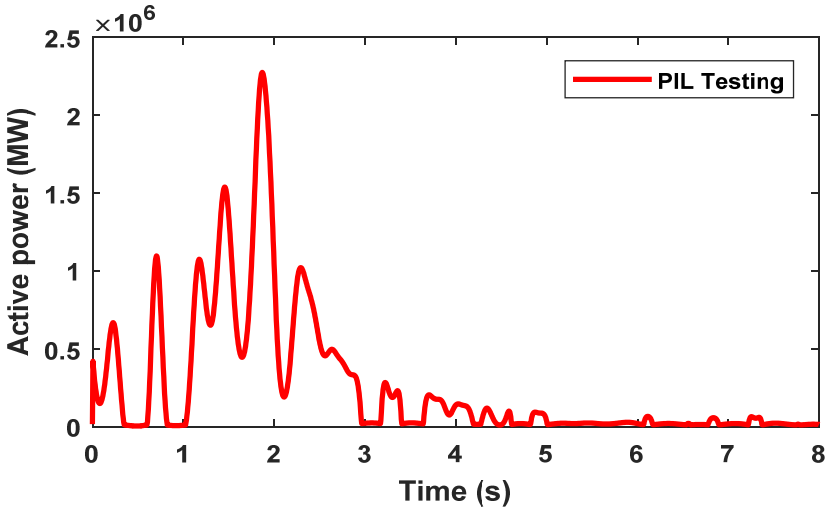

Figure 23. Active power.

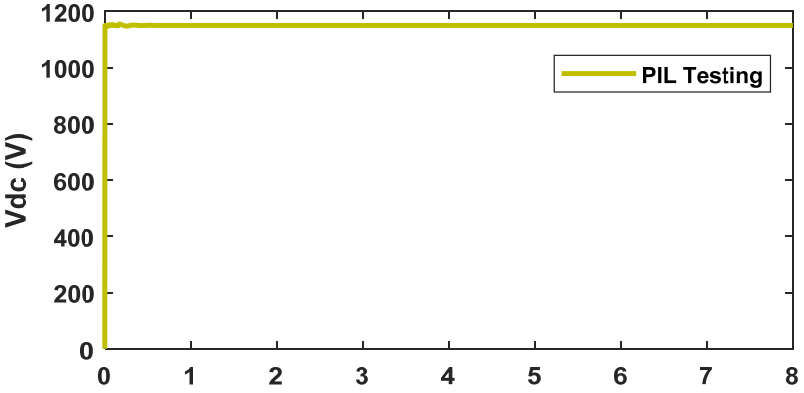

Figure 24. Experimental DC-link voltage.

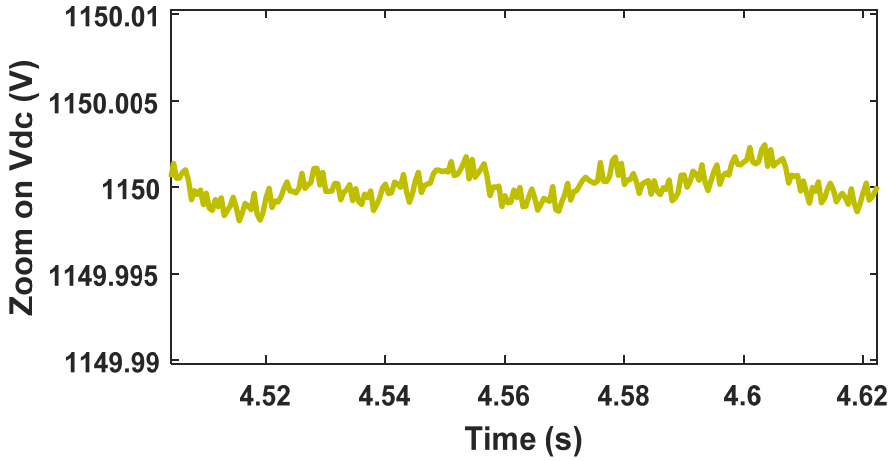

Figure 25. Zoom on the experimental DC-link voltage.

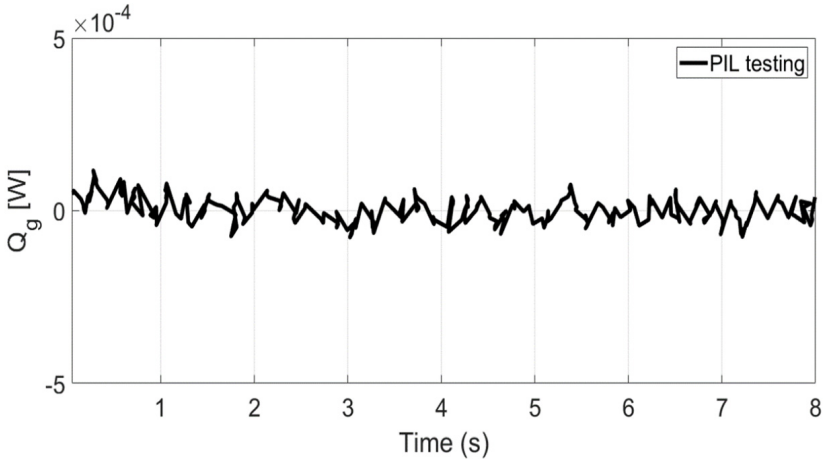

Figure 26. Experimental Reactive power.

4. Discussion and Conclusions

A novel passivity-based speed control (PBSC) combined with the fuzzy logic control for optimal performance of a PMSG is proposed for the improvement of the power quality transferred to the grid. The PBSC was adopted to design the controller law, in order to guarantee a fast convergence of the closed-loop system. The proposed strategy extracts the maximum power from the tidal energy where the entire dynamics of the PMSG is considered when designing the control law. The fuzzy logic controller is selected, which makes the proposed strategy intelligent to compute the damping gains to make the closed-loop passive and approximate the unstructured dynamics of the PMSG and thus, the robustness property of the closed-loop system is considerably increased. Dynamic simulations of the studied system under parameter changes have been given special attention and the results have been compared to nonlinear control methods, which show a quick track of the reactive power and the DC-link voltage to their references over the compared controls. Moreover, it is observed that the closed-loop operates at maximum power and integrates efficient electrical power into the grid.

From the tracing response, it can be seen that the DC voltage error is extremely reduced in the case of the proposed FS-PBSC, $\pm 1.5 \times 10^{-5}$ is observed with the lowest undershoot and overshoot. Moreover, the lowest steady-state error and better convergence criterion are shown by the proposed FS-PBSC (0.3×10^{-3} s). Generally, the proposed candidate offers high robustness, fast speed convergence, and high efficiency over the other benchmark nonlinear strategies. A comparative analysis of the proposed FS-PBSC with the other control strategies under disturbances and parameter changes performed

exhibits an ε (V_{dc}) tracking error of ±0.002 and clearly offers superior speed tracking error ε (Q_g) of ±0.000015. From the presented results, the proposed strategy clearly offers a constant voltage error V_{dc} and superior tracking error speed ε (Q_g) as compared to the other candidates, which are sensitive to the imposed disturbances.

Moreover, a PIL experiment was conducted to prove that the proposed controller is practically implementable, and from the experimental results collected using the PIL method for Tem, active power, DC-link voltage, and reactive power, respectively, it is very obvious that the proposed strategy is applicable practically.

Author Contributions: Conceptualization, Y.B. and N.U.; methodology, A.A.A.A.; software, Y.B.; validation, Y.B., N.U. and A.A.A.A.; formal analysis, A.A.A.A.; investigation, A.A.A.A.; resources, Y.B.; data curation, Y.B.; writing—original draft preparation, Y.B.; writing—review and editing, N.U. and A.A.A.A. visualization, N.U.; supervision, N.U.; project administration, A.A.A.A.; funding acquisition, N.U. and A.A.A.A. All authors have read and agreed to the published version of the manuscript.

Funding: This research was supported by TAIF University Researchers Supporting Project number (TURSP-2020/121), Taif University, Taif, Saudi Arabia.

Institutional Review Board Statement: Not applicable.

Informed Consent Statement: Not applicable.

Data Availability Statement: Not applicable.

Acknowledgments: This research was supported by Taif University Researchers Supporting Project number (TURSP-2020/121), Taif University, Taif.

Conflicts of Interest: The authors declare no conflict of interest.

References

1. Belkhier, Y.; Achour, A. Passivity-based Voltage Controller for Tidal Energy Conversion System with Permanent Magnet Synchronous Generator. *Int. J. Control Autom. Syst.* **2021**, *19*, 988–998. [CrossRef]
2. Mohammadi, E.; Fadaeinedjad, R.; Nadji, H.R. Design, electromechanical simulation, and control of a variable speed stall-regulated PMSG-based wind turbine. *Int. J. Green Energy* **2019**, *16*, 890–900. [CrossRef]
3. Wang, S. Wang Adaptive fuzzy robust control of PMSM with smooth inverse based dead-zone compensation. *Int. J. Control Autom. Syst.* **2020**, *14*, 378–388. [CrossRef]
4. Chen, H.; Tang, S.; Han, J.; Tang, T.; Ait-Ahmed, N.; Zhou, Z.; Benbouzid, M. High-order sliding mode control of a doubly salient permanent magnet machine driving marine current turbine. *J. Ocean Eng. Sci.* **2020**, *16*, 12–20. [CrossRef]
5. Othman, A.M. Enhancement of tidal generators by superconducting energy storage jaya-based sliding-mode controller. *Int. J. Energy Res.* **2020**, *44*, 11658–11675. [CrossRef]
6. Yin, X.; Zhao, X. ADV Preview based nonlinear predictive control for maximizing power generation of a tidal turbine with hydrostatic transmission. *IEEE Trans. Energy Convers.* **2019**, *34*, 1781–1791. [CrossRef]
7. Yin, X.; Zhao, X. Optimal power extraction of a two-stage tidal turbine system based on backstepping disturbance rejection control. *Int. J. Electr. Power Energy Syst.* **2021**, *132*, 107158. [CrossRef]
8. Zhou, Z.; Elghali, B.S.; Benbouzid, M.E.H.; Amirat, Y.; Elbouchikhi, E.; Feld, G. Tidal stream turbine control: An active disturbance rejection control approach. *Ocean Eng.* **2020**, *202*, 107190. [CrossRef]
9. Sahu, P.C.; Baliarsingh, R.; Prusty, R.C.; Panda, S. Novel DQN optimized tilt fuzzy cascade controller for frequency stability of a tidal energy based AC Microgrid. *Int. J. Ambient Energy* **2020**, 1–13. [CrossRef]
10. Toumi, S.; Elbouchikhi, E.; Amirat, Y.; Benbouzid, M.; Feld, G. Magnet failure-resilient control of a direct-drive tidal turbine. *Ocean Eng.* **2019**, *187*, 106207. [CrossRef]
11. Gaamouche, R.; Redouane, A.; El Harraki, I.; Belhorma, B.; El Hasnaoui, A. Optimal feedback control of nonlinear variable-speed marine current turbine using a Two-Mass model. *J. Mar. Sci. Appl.* **2020**, *19*, 83–95. [CrossRef]
12. Moon, S.H.; Park, B.G.; Kim, J.W.; Kim, J.M. Maximum power-point tracking control using perturb and observe algorithm for tidal current generation system. *Int. J. Precis. Eng. Manuf.-Green Technol.* **2020**, *7*, 849–858. [CrossRef]
13. Bhatti, M.M.; Alamri, S.; Ellahi, R.; Abdelsalam, S.I. Intra-uterine particle–fluid motion through a compliant asymmetric tapered channel with heat transfer. *J. Therm. Anal. Calorim.* **2020**, *144*, 2259–2267. [CrossRef]
14. Tamalouzt, S.; Belkhier, Y.; Sahri, Y.; Bajaj, M.; Ullah, N.; Chowdhury, M.S.; Titseesang, T.; Techato, K. Enhanced Direct Reactive Power Control-Based Multi-Level Inverter for DFIG Wind System under Variable Speeds. *Sustainability* **2021**, *13*, 9060. [CrossRef]
15. Sadaf, H.; Abdelsalam, S.I. Adverse effects of a hybrid nanofluid in a wavy non-uniform annulus with convective boundary conditions. *RSC Adv.* **2020**, *10*, 15035–15043. [CrossRef]

16. Yang, B.; Wu, Q.H.; Tiang, L.; Smith, J.S. Adaptive passivity-based control of a TCSC for the power system damping improvement of a PMSG based offshore wind farm. In Proceedings of the IEEE International Conference on Renewable Energy Research and Applications ICRERA, Madrid, Spain, 20–23 October 2013; pp. 1–5.
17. Belkhier, Y.; Achour, A.Y. Fuzzy passivity-based linear feedback current controller approach for PMSG-based tidal turbine. *Ocean Eng.* **2020**, *218*, 108156. [CrossRef]
18. Achour, A.Y.; Mendil, B.; Bacha, S.; Munteanu, I. Passivity-based current controller design for a permanent-magnet synchronous motor. *ISA Trans.* **2009**, *48*, 336–346. [CrossRef]
19. Yang, B.; Yu, H.; Zhang, Y.; Chen, J.; Sang, Y.; Jing, L. Passivity-based sliding-mode control design for optimal power extraction of a PMSG based variable speed wind turbine. *Renew. Energy* **2018**, *119*, 577–589. [CrossRef]
20. Subramaniam, R.; Joo, Y.H. Passivity-based fuzzy ISMC for wind energy conversion systems with PMSG. *IEEE Trans. Syst. Man Cybern. Syst.* **2019**, *51*, 2212–2220. [CrossRef]
21. Yang, B.; Yu, T.; Shu, H.; Qiu, D.; Zhang, Y.; Cao, P.; Jiang, L. Passivity-based linear feedback control of permanent magnetic synchronous generator-based wind energy conversion system: Design and analysis. *IET Renew. Power Gener.* **2018**, *12*, 981–991. [CrossRef]
22. Khanchoul, M.; Hilairet, M.; Normand-Cyrot, D. A passivity-based controller under low sampling for speed control of PMSM. *Control Eng. Pract.* **2014**, *26*, 20–27. [CrossRef]
23. Liu, X.; Yu, H.; Yu, J.; Zhao, Y. A novel speed control method based on port-controlled hamiltonian and disturbance observer for PMSM drives. *IEEE Access* **2019**, *7*, 111115–111123. [CrossRef]
24. RWang, L.; Lu, B.C.; Hou, Y.L.; Gao, Q. Passivity-based control for rocket launcher position servo system based on ADRC optimized by IPSO-BP Algorithm. *Shock. Vibr.* **2018**, *2018*, 5801573.
25. Khefifi, N.; Houari, A.; Machmoum, M.; Ghanes, M.; Ait-Ahmed, M. Control of grid forming inverter based on robust IDA-PBC for power quality enhancement. *Sustain. Energy Grids Netw.* **2019**, *20*, 100276. [CrossRef]
26. Belkhier, Y.; Achour, A.Y. An intelligent passivity-based backstepping approach for optimal control for grid-connecting permanent magnet synchronous generator-based tidal conversion system. *Int. J. Energy Res.* **2020**, *45*, 5433–5448. [CrossRef]
27. Espinosa-Perez, G.; Godoy-Alcantar, M.; Guerrero-Ramfrez, G. Passivity-based control of synchronous generators. In Proceedings of the ISIE'97 IEEE International Symposium on Industrial Electronics, Guimaraes, Portugal, 7–11 July 1997; Volume 1, pp. SS101–SS106. [CrossRef]
28. Nicklasson, P.J.; Ortega, R.; Espinosa-Perez, G. Passivity-based control of the general rotating electrical machine. In Proceedings of the 1994 33rd IEEE Conference on Decision and Control, Lake Buena Vista, FL, USA, 14–16 December 1994; Volume 4, pp. 4018–4023. [CrossRef]
29. Lee, M.A.; Takagi, H. Dynamic control of genetic algorithms using fuzzy logic techniques. In Proceedings of the International Conference on Genetic Algorithms, Urbana-Champaign, IL, USA, 1 June 1993; pp. 76–83.
30. Yubazaki, N.; Otami, M.; Ashid, T.; Hirota, K. Dynamic fuzzy control method and its application to positioning of induction motor. In Proceedings of the Fourth IEEE International Conference on Fuzzy Systems, Yokohama, Japan, 20–24 March 1995; pp. 1095–1102.
31. Belkhier, Y.; Achour, A.; Shaw, R.N.; Ullah, N.; Chowdhury, M.S.; Techato, K. Fuzzy Supervisory Passivity-Based High Order-Sliding Mode Control Approach for Tidal Turbine-Based Permanent Magnet Synchronous Generator Conversion System. *Actuators* **2021**, *10*, 92. [CrossRef]
32. Ullah, N.; Farooq, Z.; Sami, I.; Chowdhury, M.S.; Techato, K.; Alkhammash, H.I. Industrial Grade Adaptive Control Scheme for a Micro-Grid Integrated Dual Active Bridge Driven Battery Storage System. *IEEE Access* **2020**, *8*, 210435–210451. [CrossRef]
33. Ullah, N.; Sami, I.; Chowdhury, M.S.; Techato, K.; Alkhammash, H.I. Artificial Intelligence Integrated Fractional Order Control of Doubly Fed Induction Generator-Based Wind Energy System. *IEEE Access* **2021**, *9*, 5734–5748. [CrossRef]
34. Ullah, N.; Ullah, A.; Ibeas, A.; Herrera, J. Improving the Hardware Complexity by Exploiting the Reduced Dynamics-Based Fractional Order Systems. *IEEE Access* **2017**, *5*, 7714–7723. [CrossRef]